JOURNAL OF GEOPHYSICAL RESEARCH, VOL. 107, NO. C21, 8043, doi:10.1029/2000JC000409, 2002

Thermal conductivity and heat transfer through the snow on the ice of the Beaufort Sea

Matthew Sturm
U.S. Army Cold Regions Research & Engineering Laboratory-Alaska, Fort Wainwright, Alaska, USA

Donald K. Perovich
U.S. Army Cold Regions Research & Engineering Laboratory, Hanover, New Hampshire, USA

Jon Holmgren
U.S. Army Cold Regions Research & Engineering Laboratory-Alaska, Fort Wainwright, Alaska, USA

Received 2 May 2000; revised 24 February 2001; accepted 23 July 2001; published 10 October 2002.

[1] Eighty-nine point measurements of the thermal conductivity (k_s) of the snow on the sea ice of the Beaufort Sea were made using a heated needle probe. Average values ranged from 0.078 W m^{-1} K^{-1} for new snow to 0.290 W m^{-1} K^{-1} for an ubiquitous wind slab. k_s increased with increasing density, consistent with published equations, but could also be reliably estimated from the metamorphic state of the snow. Using measured values of k_s and snow stratigraphy, the average bulk value for the full snowpack was 0.14 W m^{-1} K^{-1}. In contrast, k_s inferred from ice growth and temperature gradients in the snow was 0.33 W m^{-1} K^{-1}. The mismatch arises in part because the second estimate is based on measurements from an aggregate scale that includes enhanced heat flow due to two- and three-dimensional snow and ice geometry. A finite element model suggests that the complex geometry produces areas of concentrated heat loss at the snow surface. These "hot spots," however, increase the apparent conductivity only by a factor of 1.4, not enough to fully explain the mismatch. Nonconductive heat transfer mechanisms, like natural and forced air convection, may also be operating in the snowpack, though the ubiquitous presence of low permeability wind slabs potentially limits their effectiveness. The relative contributions of effects due to snow and ice geometric and nonconductive processes within the snowpack remain uncertain. *INDEX TERMS:* 1863 Hydrology: Snow and ice (1827); 4207 Oceanography: General: Arctic and Antarctic oceanography; 4540 Oceanography: Physical: Ice mechanics and air/sea/ice exchange processes; *KEYWORDS:* snow, snow cover, Arctic ocean, thermal conductivity, heat flow, sea ice

Citation: Sturm, M., D. K. Perovich, and J. Holmgren, Thermal conductivity and heat transfer through the snow on the ice of the Beaufort Sea, *J. Geophys. Res.*, *107*(C21), 8043, doi:10.1029/2000JC000409, 2002.

1. Introduction

[2] Without direct measurements, researchers studying energy exchange over the Arctic ice pack have had to use estimates of the thermal conductivity of the snow (k_s) based regression equations relating k_s to snow density (ρ_s). These equations have been established for snow that was not on sea ice. Thermal conductivity, however, is a function of snow texture (e.g., grain size, shape, and bonding) as well as density [*Mellor*, 1977; *Sturm et al.*, 1997], and texture is known to vary with substrate: the past estimates of k_s may be inaccurate. Unfortunately, this density-based approach has been the only choice up until now. Snow density measurements have been widely available for the Arctic Ocean [*Vowinkel and Orvig*, 1970; *Radionov et al.*, 1997; *Colony et al.*, 1998; *Warren et al.*, 1999], but textural descriptions and thermal conductivity measurements have not. Here, we report on new, direct measurements of k_s made on the snow covering the sea ice of the Beaufort Sea. These were made during project SHEBA (*S*urface *HE*at *B*udget of the *A*rctic Ocean) [*Perovich et al.*, 1999], and a search of the literature suggests they may be the first such measurements from the Arctic Ocean. Using the new measurements, we examine if the old estimates are in need of revision.

[3] That assessment is not as simple as it might seem. The sea ice and snow system is extremely heterogeneous. The layered nature of the snowpack produces large vertical variations in thermal properties, and the thickness of both ice and snow layers varies over short distances (Figure 1). All of these variations evolve and change continually throughout the winter due to ice growth and deformation, snowfall, and drifting. Making enough measurements, both vertically and horizontally, to derive temporally and spatially representative bulk thermal conductivity values is

0148-0227/02/2000JC000409$09.00

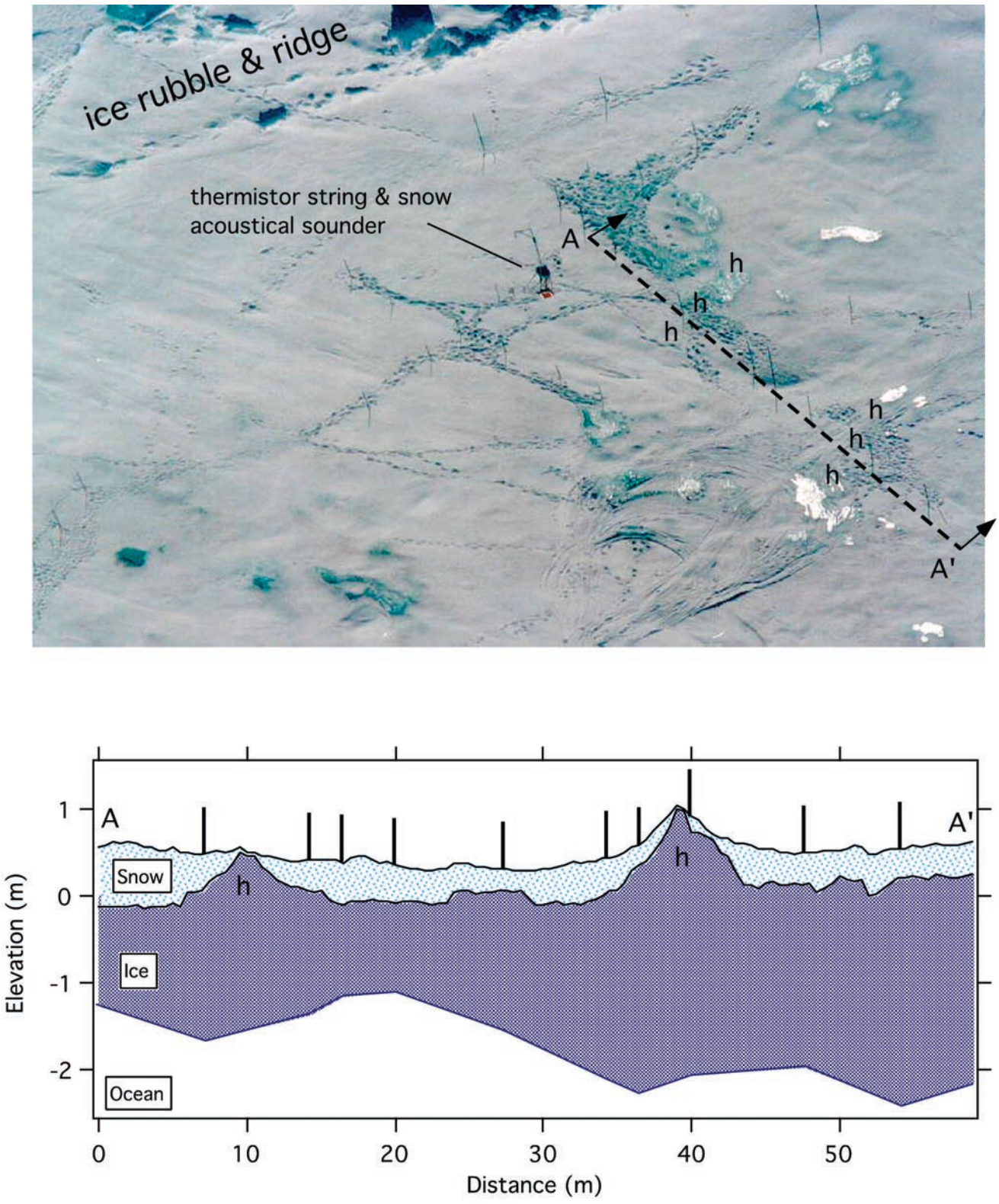

Figure 1. The ''Seattle'' research site at SHEBA in mid-June when melting had exposed variations in the snow cover and made apparent the heterogeneity of the snow and ice system. The location of the cross section (A-A′) is shown by the heavy dashed line; snow/ice stakes appear in the photograph as faint vertical lines. The footprints were made in June after the melt had softened the snow.

difficult, if not impossible. Here, we have tried to overcome this difficulty by relating measurements of k_s to the snow stratigraphy, which was more easily observed, but ultimately we have undersampled the system.

[4] As a further complication, our 89 measurements are essentially point values made on bench-top-sized samples of snow, while surface energy balance models tend to be applied at much larger scales. As we show here, heat transfer across the sea ice and snow at these larger scales is probably not a one-dimensional vertical process, despite the fact that it is always modeled as one. It is almost certainly three-dimensional and highly complicated, with heat flow enhancement occurring in selected locations. k_s-values needed to balance the surface energy budget probably vary with size of the area of interest, and are related only in a complex way to point measurements. This scale-dependent behavior arises because snow is one of the best insulating materials found in nature. Where the snow is thicker, the resistance to heat flow is higher and heat tends to flow elsewhere. This creates lateral as well as vertical heat flow paths, and leads to the development of areas of concentrated heat loss at the snow and ice surface.

2. Location

[5] The SHEBA camp was established on the ice of the Beaufort Sea at 75°N, 142°W in early October 1997 and then drifted until October 1998 at which time it had reached 80°N, 162°W [*Perovich et al.*, 1999]. About 11 cm of snow was already on the ice in October 1997 when the project began. The snowpack continued to build, rapidly between October and early December, and then more slowly until spring. In April and May, when the pack had reached maximum depth, we made detailed measurements of snow depth, density, stratigraphy, and thermal conductivity [*Sturm et al.*, 2002]. Throughout the winter we monitored snow and ice temperature and thickness at several sites [*Perovich and Elder*, 2001].

3. Methods

3.1. Thermal Conductivity

[6] Snow thermal conductivity was measured using a needle probe described by *Sturm* [1991], *Sturm and Johnson* [1991], and *Sturm et al.* [1997]. Some of the measurements at SHEBA were made on snow samples that were cut from the snow cover, boxed, and removed to the camp where they were stored until they were isothermal. Others were made in situ in the walls of snow pits. The measurements were keyed to the ten layers of snow that made up the snowpack.

[7] Studies [*Pratt*, 1969; *Presley and Christensen*, 1997] have shown that for low conductivity and granular materials (snow fits both categories), a dynamic heating and cooling test using a needle probe is one of the best methods for measuring the thermal conductivity. Alternate methods that have been used on snow include calculation of k_s from in situ temperatures [*Abel*'s, 1893], and using a guarded hot plate [*Pitman and Zuckerman*, 1967]. Values of k_s based on in situ temperature measurements probably include heat transfer by nonconductive processes (i.e., convection or solar heating) and the derived values are probably too high. Guarded hot plate methods have proved difficult to use on snow because (1) it can take several days to bring a sample into steady state, during which time the snow undergoes metamorphism, and (2) the strong temperature gradients that need to be imposed on a sample result in the migration of water vapor and frost build-up on the cold plate of the apparatus, biasing the results.

[8] Our needle probe (Soiltronics model TC1 modified) was 1.5 mm in diameter and 20 cm long, but heated only over the distal 12 cm. The probe, which contained a helical heating wire with a thermocouple located within the helix, was inserted into a snow sample, then heated for 3 min during which its temperature was measured every 0.5 s. It was then allowed to cool while its temperature was monitored for a further 7 min. The entire test was controlled and recorded using a data logger (Campbell CR-10). Thermocouple temperatures were accurate to ±0.02°C. From the full test cycle, two independent values of thermal conductivity, k_{sh} for the heating cycle, and k_{sc} for the cooling cycle, were calculated and then averaged together to produce one value of k_s. If k_{sh} and k_{sc} differed by more than 15%, both tests were discarded (12 out of 101 tests were discarded for this reason). The needle had a small diameter ferrule where the wires were attached so that needle and wire could be embedded completely in the snow sample. This, coupled with the 8 cm long unheated section, reduced end effects that normally adversely affect the accuracy of needle probe measurements [cf. *Blackwell*, 1956].

[9] The theory behind the probe's operation has been widely discussed [*Jaeger*, 1956, 1958; *Lachenbruch*, 1957], and probes have been used to make measurements in snow for 30 years [*Jaafar and Picot*, 1970; *Lange*, 1985; *Murakami and Maeno*, 1989; *Sturm and Johnson*, 1991]. Basically, the thermal conductivity of a material (k) in which a needle is embedded is proportional to the rate the needle is heated and the natural log of the elapsed time (t_1 to t_2), and inversely proportional to the rise in temperature of the needle (ΔT):

$$k_s \approx \frac{q_n}{4\pi\Delta T}\{\ln(t_2) - \ln(t_1)\} \quad (1)$$

where q_n is the rate of heat generation in the needle per unit length of the heated portion of the needle, equal to $V^2/L_n r$, with r the heater wire resistance per unit length, V the input voltage (averaged for the heating cycle), and L_n the heated length of the needle.

[10] The accuracy of the needle and controller was checked during the field campaign by making periodic measurements on a polyurethane foam ''standard'' of known thermal conductivity. Measured values (0.0172 ± 0.0012 W m^{-1} K^{-1}, n = 6) fell within 15% of the nominal value. After the conclusion of SHEBA, the thermal conductivities of several materials for which published values were available (Table 1) were measured with the same needle. These were chosen to bracket the values of snow. Because the accuracy and method used in determining some of the published values were obscure, we also measured the same materials on a commercial guarded hot plate apparatus (Holometrix Model TCFG-R4-6). The needle probe produced values that were within 3% of published values, and within 5 to 20% of the commercial guarded hot plate values. In most cases, needle probe values were closer than hot plate

Table 1. Comparison of Needle Probe Values to Published and Guarded Hot Plate Values for Several Materials

	[W m^{-1} K^{-1}]
Polyurethane foam	
April 1997 (during SHEBA) (n = 6)	0.0172
September 1999 (after SHEBA) (n = 3)	0.0170
Published value	0.0163
Hot plate test (Anacon) (n = 2)	0.0180
Glycerol	
August 1999 (n = 3)	0.2888
September 1999 (n = 1)	0.2980
Published value [*Touloukian et al.*, 1970]	0.2880 ± 0.03
Styrofoam	
September 1999 (n = 5)	0.0259
Manufacturer's published value (ASTM Method C518)	0.0272 ± 0.0015
Guarded hot plate test (Holometrix) (n = 3)	0.0330
Water (distilled) stabilized with 0.04%agar	
February 1999 (n = 5)	0.613
Published value [*Lide*, 1997]	0.609

values to the published value. We conclude that the values of k_s we report here are accurate to ±0.005 W m^{-1} K^{-1}.

[11] We also investigated whether conditions during the needle probe tests differed from those found in a natural snow cover in such a way as to bias the test results. In snow, in the absence of convection, heat transfer takes place in four ways: radiation from one snow grain to another, conduction through the ice grains, conduction across air spaces, and vapor diffusion from grains at higher temperatures to those at lower temperatures. Radiation heat transfer is negligible and the conduction of heat across air spaces is small in comparison to that across ice grains (roughly 1:100), leaving conduction through the ice skeleton and vapor transport as the main mechanisms for heat transfer. For a snow sample in a guarded hot plate apparatus, a steady state, one-dimensional vapor transport system develops. In a needle probe test, a transient vapor transport system develops along with the transient temperature field. Vapor transport in a natural snow cover falls somewhere between the two, with snow layers higher in the pack subjected to ambient fluctuations in air temperature and more transient conditions for vapor transport, while layers lower in the pack are buffered in temperature by the overlying layers of snow, approximating a steady state vapor transport system. Even if the test and natural systems differ, three studies [*DeVries*, 1958; *DeVries and Peck*, 1958; *Ewen and Thomas*, 1987] suggest that needle probe measurements should be fully applicable to both steady state and transient heat flow situations, even when vapor transport is important.

3.2. In Situ Snow and Ice Temperatures

[12] Hourly measurements of the temperature in the snow and ice were recorded at 6 locations at SHEBA [*Perovich and Elder*, 2001]. At each site a 3.2 cm diameter PVC rod with thermistors (YSI#44033; ±0.1°C) mounted flush with the outer surface was inserted in a hole drilled into the ice and allowed to freeze in. After the initial disturbance due to installation, snow accumulated naturally around the rod. Here, we use primarily the data from the "Seattle" site where a rod extended 1.5 m down into the ice and 1.0 m above, with thermistors every 0.1 m. In addition, we use data from an additional 30 locations where thermistors accurate to ±1.0°C (cf. http://arcss.colorado.edu/Catalog/arcss001.html) [*Sturm et al.*, 2001] were installed at the snow–ice interface and attached to minidata loggers (Hobo-XT, Onset Computer Corp., see http:/www.onsetcomp.com). At these locations, temperatures were recorded every 2.4 hours throughout the winter and local snow depth and ice thickness were recorded weekly. We use these temperature and snow and ice thickness data to compute the heat flux through the ice and snow. Measurements of snow depth and ice thickness were accurate to about ±0.02 m.

3.3. Other Measurements

[13] In April and May, and snow layer characteristics and densities were measured at 194 locations [*Sturm et al.*, 2002]. The layers, natural units of the snowpack, were deposited by storm and wind events. Each layer tended to have homogeneous and recognizable density and grain characteristics, but wide variations in thickness. The layers were classified into one of 15 types of snow (Table 2) based on inspection, with type codes chosen so that increasing values corresponded roughly with increasing degrees of metamorphism. Layer "hardness" was ascertained by resistance to penetration by a fist, several fingers, a pencil or knife, in accordance with the International Classification of Snow on the Ground [*Colbeck et al.*, 1992]. Density was measured with a 100 cm^3 stainless steel cutter and digital balance (accurate to ±0.01 g cm^{-3}). Thermal conductivity measurements were keyed to individual layers.

4. Results

[14] There were three major types of snow (depth hoar, wind slab, and recent) in ten layers at SHEBA (Figure 2). We made thermal conductivity measurements on approximately 10% of all layers on which we measured density, hardness and type (Table 3). This thermal subset was slightly more dense and a little harder than the snow in the full set (Table 3), reflecting a natural bias toward layers, that were easier to test. Five of the 10 layers of snow ("a", "b", "d", "g", and "j") were undersampled, while two layers ("c" and "f") were oversampled (compare % *of total snowpack* to % *of total samples* in Table 3), but these biases are

Table 2. Snow Type Codes Used at SHEBA[a]

Snow type	Code
new	1
recent	2
fine-grained snow	3
medium-grained snow	4
soft wind slab	5
moderately hard slab	6
hard wind slab	7
very hard wind slab	8
wind slab turning to depth hoar	9
depth hoar	10
vertical chains of depth hoar	11
chains of depth hoar, indurated	12
chains of depth hoar with large voids	13
icy depth hoar	14
snow ice	15

[a] See the International Classification for Snow on the Ground [*Colbeck et al.*, 1992] for full descriptions of each type.

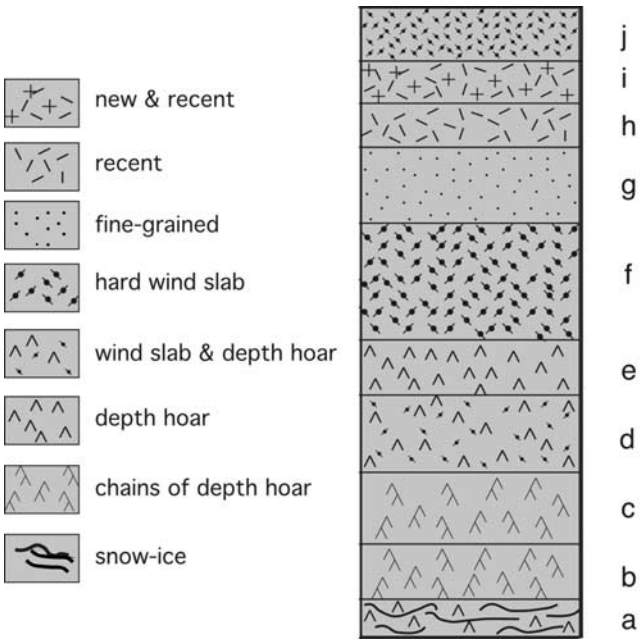

Figure 2. Snow stratigraphy at SHEBA in April 1998. See the *Sturm et al.* [2002] reference for more details.

unimportant because (later) we use a layer-weighted averaging method to derive a bulk value of k_s for the whole snowpack.

[15] The average layer values of k_s (Table 3) varied from 0.078 to 0.574 W m^{-1} K^{-1}, with the highest value for a layer of snow ice (layer "a"), and the lowest value for a layer of newly deposited snow (layers "h" and "i" combined). For nonicy snow, the highest value (0.290 W m^{-1} K^{-1}) was for layer "f", a ubiquitous, hard wind slab.

[16] Snow texture may be a more "model-friendly" predictor of k_s than density for snow on sea ice, but $k_s - \rho$ regressions are in wide use, so we have compared the SHEBA data to previous work. Layer average values of k_s increased smoothly with layer density (ρ) (Figure 3) consistent with regression equations suggested by *Sturm et al.* [1997]:

$$k_s = 0.138 - 1.01\rho + 3.233\rho^2 \qquad \{0.156 \le \rho \le 0.6\} \qquad (2a)$$

$$k_s = 0.023 - 1.01\rho + 0.234\rho^2 \qquad \{\rho < 0.156\} \qquad (2b)$$

but fell below the regression equation of *Abel*'s [1893] for reasons discussed later. Conductivity values for snow ice (measured at SHEBA) and sea ice were also predicted correctly using equation (2a).

[17] A less orderly picture emerges if all k_s-data (Appendix A) are plotted (Figure 3 inset) instead of just layer averages. The high scatter in these data (see also SD of k_s in Table 3) reflect real spatial variations in layer properties. For example, layer "c", a depth hoar layer, had k_s-values ranging from 0.04 to 0.16 W m^{-1} K^{-1} and densities that varied from 0.21 to 0.33 g cm^{-3}. This spatial variability is highlighted by the wide variation in hardness exhibited by each layer. While average values of k_s increased as smoothly with hardness (Figure 4), the histograms in the figure document that for each hardness value between 1 and 4, virtually every layer was represented. Layer "f", the thickest and densest slab in the pack, generally had hardness values of 3 or more, but an appreciable number of f-layer samples fell in hardness classes 1 or 2. This high spatial variability in layer properties was the result of wind transport and drifting.

[18] Statistical analysis indicates that 87% of the variance in k_s can be explained if all three explanatory variables, density, hardness, and snow type, are used together. Hardness and density, which are highly correlated (r^2 = 0.77), explain about 85% and 83% of the variance, respectively, if used individually, and no more than 85% if used together. The slightly higher value for hardness arises because bonding between snow grains affects both thermal conductivity and snow strength alike, while density is a slightly less direct measure. Perhaps with a more precise way of measuring the hardness, it would have proven the most efficient and best predictor of thermal conductivity, since the measurement can be made quickly. Snow type, also easily measured, predicted only about 75% of the variance of k_s. While this is the lowest percentage of all three explanatory variables, it is nearly as high as the value for density (the commonly used predictor) and snow class may be the most tractable variable to simulate in models. Computer codes like CROCUS and SNTHERM are already available [*Jordan*, 1991; *Brun et al.*, 1992] and these can be used to predict snow metamorphism and snow type or class from atmospheric forcing.

[19] By plotting k_s as a function of snow type (Figure 5), the SHEBA data define in a general way the evolution of the thermal conductivity of a snow layer through the winter. This

Table 3. Layer Average Values of Thermal Conductivity, Density, SWE and Hardness for All Snow Pits and Thermal Conductivity Samples Only

Layer	All snow layers				Thermal conductivity samples				
	n	Density, g cm^{-3}	Hardness (index)	% of total snow pack	*n*	% of total samples	density, g cm^{-3}	k_s, W m^{-1} K^{-1}	SD of k_s, W m^{-1} K^{-1}
J	11	0.32	2.6	9%	3	3%	0.39	0.203	0.004
h & i	199	0.19	1.2	5%	5	6%	0.20	0.078	0.024
G	103	0.32	2.4	13%	8	9%	0.36	0.197	0.081
F	201	0.40	3.9	26%	29	33%	0.42	0.290	0.124
E	3	0.28	3.0	<1%	3	3%	0.28	0.157	0.012
D	85	0.34	3.2	16%	8	9%	0.36	0.164	0.081
C	182	0.28	2.3	11%	22	25%	0.27	0.081	0.039
B	102	0.34	3.1	11%	3	3%	0.27	0.087	0.069
A	9	0.51	5.3	9%	1	1%	0.60	0.574	–
ridge drift	6	0.35	3.0	–	7	7%	0.35	0.146	0.015

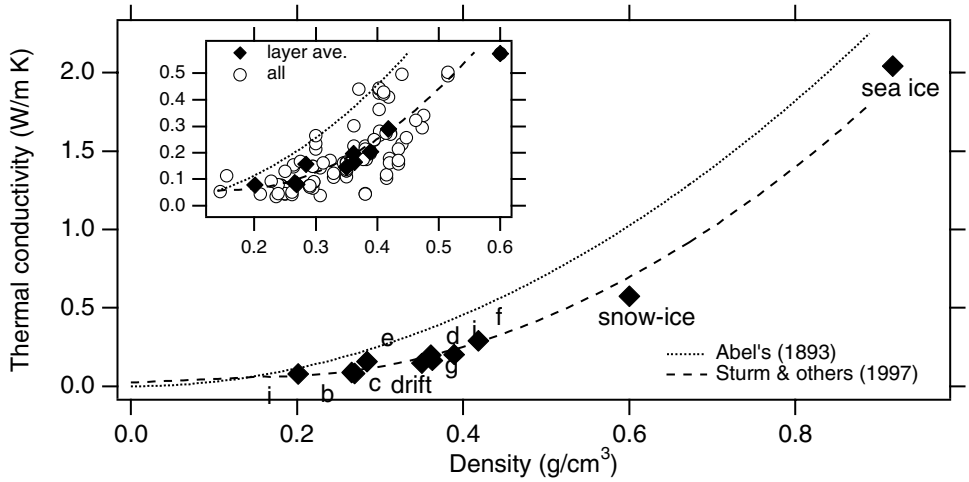

Figure 3. Average layer k_s-values as a function of average layer density. Regression equations of k_s versus density from the works of *Sturm et al.* [1997] and *Abel*'s [1893] are shown. The inset shows individual as well as layer values.

procedure is possible because the stratigraphic sequence of layers in the pack is also a rough analog for the temporal evolution of a single layer. In the absence of wind, low-density new snow is deposited with a correspondingly low initial value of thermal conductivity. The layer immediately begins to compact and settle, increasing in density and bonding. As this occurs, the value of k_s rises (Figure 5). At this point, if the fine-grained snow is transported by the wind, grains will be pulverized and their size reduced further. When the drifting grains come to rest, a wind slab will form through sintering, producing a dramatic rise in slab hardness and k_s. The higher the wind speed, the denser and harder the slab, and the higher the value of k_s. Once deposited, the slab will start to metamorphose into depth hoar due to the strong temperature gradients imposed upon it. These arise because ambient air temperatures are low, but ice surface temper-

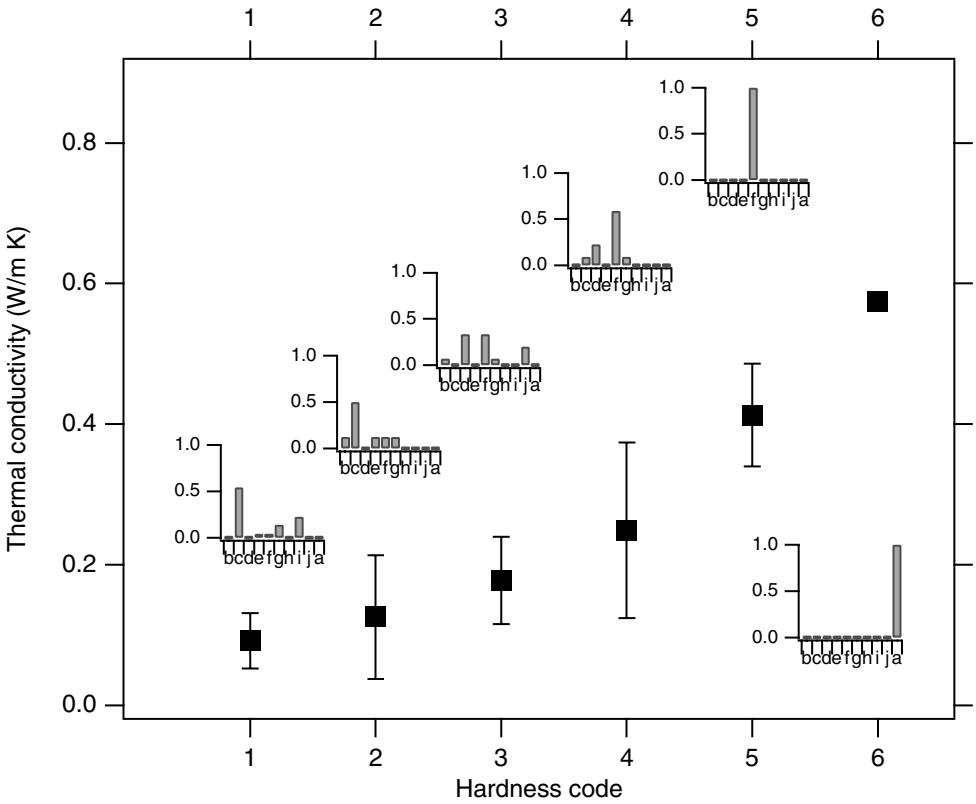

Figure 4. Layer k_s-values versus hardness for data. Hardness scale (qualitative) is based on the penetration resistance of the snow: 1 = fist, 2 = four fingers, 3 = one finger, 4 = pencil, 5 = knife, and 6 = icy. Error bars indicate ± one standard deviation. Small letters under histograms refer to layers in Figure 2.

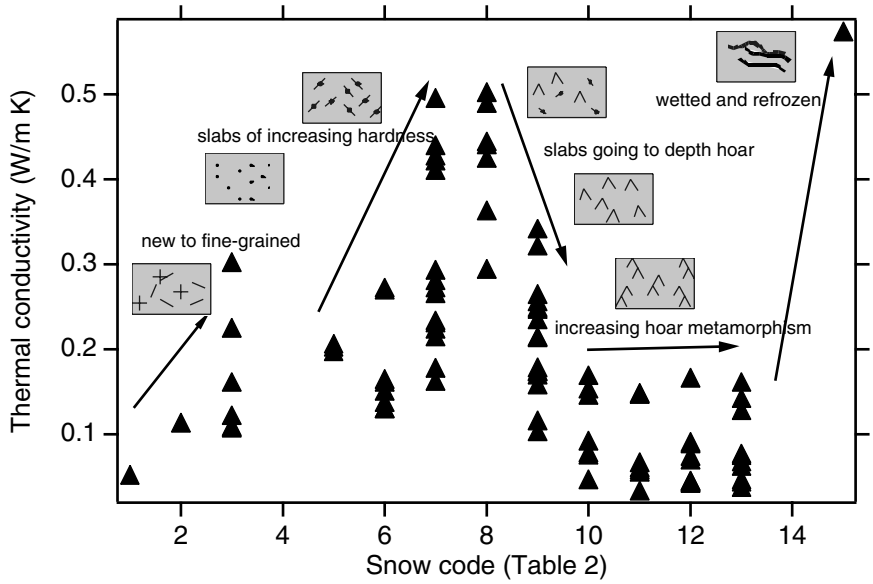

Figure 5. Thermal conductivity trajectories based on k_s-values and sample descriptions from SHEBA. Snow symbols are the same as in Figure 2.

atures are high. Initially, a slight weakening accompanying a limited amount of kinetic crystal growth will occur, with a corresponding limited reduction in k_s. With more time, vigorous depth hoar metamorphism will reduce the hardness of the layer dramatically through an increase in crystal size and a reduction in the number and thickness of bonds. Values of k_s will reduced and approach the values associated with new snow. Finally, in spring, the layer may undergo melting and refreezing, producing icy features and much higher values of k_s. Not all layers will follow all legs of the trajectory shown in Figure 5, but if the snow type or class can be estimated, values of thermal conductivity can be assigned.

5. Bulk Conductivity From Probe Measurements and Snow Pits

[20] We can extrapolate the k_s sample and layer measurements to the snow cover that blanketed the SHEBA area in a simple fashion by using the snow pit data. We use measured snow layer thickness and assume vertical heat flow (an assumption we question shortly), calculating the bulk thermal conductivity for each snow pit (n = 194) from:

$$1/k_{s,bulk} = \sum_{i=1}^{n} \frac{\phi_i}{k_{si}} \tag{3}$$

where ϕ is the fraction of the total snowpack depth of the i^{th} layer, and k_{si} is the layer thermal conductivity. Our results show that k_{si} was highly variable, particularly for layers "c", "d", "f", and "g", so for each of these layers we have established a linear regression between k_{si} and density. We use the regression and the measured density to assign a value of k_{si} to each layer. For layers "a", "b", "e", "h", "i", and "j", the average k_s-values from Table 3 were used. When computed for all snow pits, the average bulk thermal conductivity at SHEBA was 0.130 ± 0.032 W m^{-1} K^{-1}.

[21] A second method of extrapolation, which makes use of the large body of depth measurements made at SHEBA, produces a similar result. The average April snow depth at SHEBA was 33.7 cm with a standard deviation of 19.3 cm (n = 21,169) [*Sturm et al.*, 2002]. Using the average fraction of the total snowpack for each layer (Table 3; all snow pits), we subdivided a 33.7 cm deep snowpack into the ten "typical" layers found at SHEBA. To each of these layers we assigned a thermal conductivity value using equation (3). The result is a snowpack with a density of 0.351 g cm^{-3}, a depth hoar fraction of 0.38, a wind slab fraction of 0.48, and a bulk k_s-value of 0.14 W m^{-1} K^{-1}. This "average" snowpack is slightly denser than the mean for all snow pits, and composed of slightly more wind slab, but overall the resulting bulk k_s-value is in good agreement with the estimate from the previous method.

6. Bulk Conductivity Inferred From Ice Growth

[22] In this section, we use the ice growth measured at SHEBA to infer the total amount of heat extracted from the ice during the winter, and from that quantity, the effective bulk thermal conductivity of the snow required to transport the heat. We contrast this inferred value with the bulk estimates derived in the previous section, finding the former to be substantially higher than the latter, and to vary with location. We think that part of the mismatch arises because of the difference in the scale of the two measurements. The needle probe measurements are effectively point values, while ice growth was measured at a scale that includes considerable heterogeneity in the snow and ice. An unstated assumption in most sea ice heat transfer models is that a bulk value of k_s derived from point measurements can be used at a variety of spatial scales. This is equivalent to the assumption that the average value of thermal conductivity used in a one-dimensional model of heat flow, applied widely, will produce realistic area-averaged heat flow estimates. But is this assumption valid, or is the heat flow dominated by extreme cases produced by lateral heat flow? Which, if any, of our derived values is the appropriate one

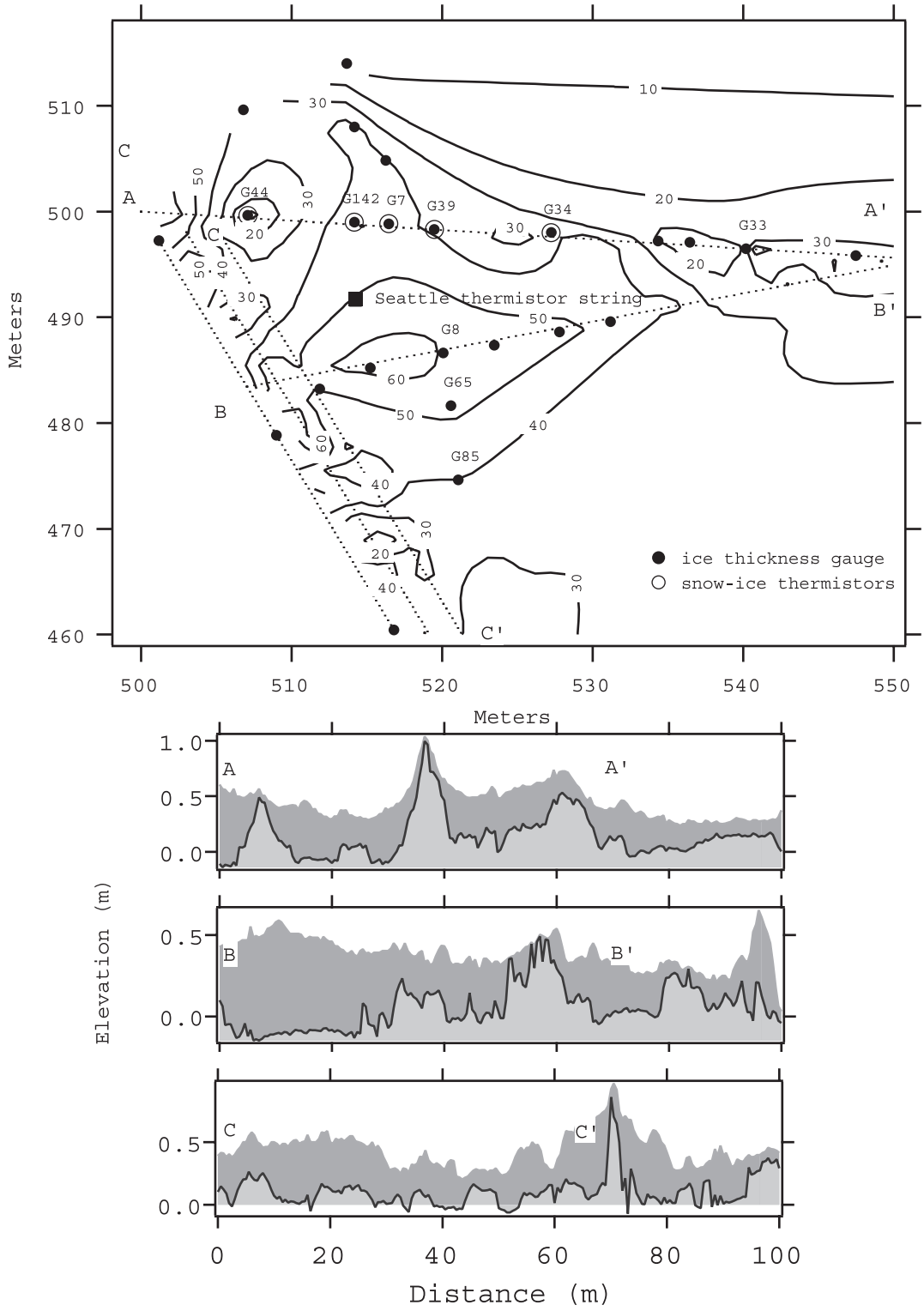

Figure 6. Seattle site map, showing stake locations, snow depth measurement points, and snow depth contours (cm). The vertical thermistor locations are shown by the solid square. Cross-section locations are marked as A-A′, B-B′, and C-C′ and shown in the lower part of the figure. Part of the A-A′ cross section also appears in Figure 1.

to use? To further complicate the problem, there is a possibility that nonconductive heat transfer mechanisms move heat in the natural snowpack on the ice but are not replicated in the needle probe test.

[23] We begin by estimating the effective value of k_s from ice growth at the "Seattle" site, our most comprehensive data set (Figures 1 and 6). At the center of the site there was a refrozen melt pond in which a thermistor string and

several ice thickness/snow depth stakes (Figure 6) were installed. Other stakes were installed in bubbly white ice hummocks adjacent to the pond and in a few smaller melt ponds nearby. Near several stakes, thermistors were placed at the snow–ice interface. The snow was deepest over the ponds and shallowest over the ice hummocks. For the ice, the converse was true: it was thinnest where there were ponds and thickest where there were hummocks.

[24] Assuming one-dimensional heat flow, the change in heat content of the snow and ice, the heat of fusion due to ice growth, the energy input due to solar heating, and the heat input to the ice from the ocean must all be extracted vertically through the snow cover. This is expressed as:

$$-\int k_s \frac{dT_s}{dz} dt = Q_{ss} + Q_{si} + Q_L + Q_w + Q_{sw}, \tag{4}$$

where dt is the time interval, z is the vertical coordinate, dT_s/dz is the temperature gradient in the snow, Q_{ss} is the specific heat of cooling the snow, Q_{si} is the specific heat of cooling the ice, Q_L is the latent heat of freezing new ice, Q_w is the heat from the ocean, and Q_{sw} is solar heat. As a practical matter, we use the average temperature gradient across the entire snowpack, in which case k_s becomes the bulk thermal conductivity of the pack, comparable to the value in equation (3).

[25] We want to estimate an average value of the snow conductivity for the winter at the Seattle thermistor string, so we assume k_s is constant in time, allowing it to be moved outside the integral. For integration limits, we choose 9 December 1997 to 8 March 1998, days when snow depth and ice thickness was measured. The start date was selected to provide ample time for recovery from the effects of installing the instruments in the snow. The end date was selected to avoid complications due to solar heating and a large transient in the ocean heat flux. Prior to March, incident solar irradiance is small and the amount absorbed in the snow and ice (Q_{sw}) can be neglected. In late March, there was a sharp increase in the ocean heat flux as ice station SHEBA drifted into shallower water [*Perovich et al.*, 1999], a complication we avoid with our choice of dates.

[26] The amount of heat extracted to cool the snow (Q_{ss}) and ice (Q_{si}) is:

$$Q_{ss} = -\rho_s c_i \int_{snow} \big(T_f(z) - T_i(z)\big) dz \tag{5a}$$

$$Q_{si} = -\rho_i c_{si} \int_{ice} \big(T_f(z) - T_i(z)\big) dz \tag{5b}$$

where f and i indicate the final and initial conditions, respectively, for the period of calculation. The constants in the equation are the snow density (ρ_s = 340 kg m^{-3}), the ice density (ρ_i = 917 kg m^{-3}), the specific heat of ice (c_i = 2.01 kJ kg^{-1} °C^{-1}), and the specific heat of sea ice (c_{si}, relationship from the work of *Schwerdtfeger* [1963]). The temperature change was computed using profiles from the thermistor string at Seattle for the period 9 December 1997 ($T_i(z)$) to 8 March 1998 ($T_f(z)$). There was little difference in the snow temperature profile at the beginning and end of the period and the specific heat change was small, with Q_{ss} equal to 1.1 MJ m^{-2}. Changes in ice temperature were greater, with Q_{si} equal to 10.5 MJ m^{-2}.

[27] The latent heat resulting from the freezing of ice was computed using:

$$Q_L = \rho_i \int q_m dz \tag{6}$$

where q_m is the amount of heat needed to freeze a unit mass of sea ice to a temperature T_o and is given by *Schwerdtfeger* [1963] and corrected by *Ono* [1967]:

$$q_m = -c_w T_f + c_i\big(T_f - T_0\big) + L\left(1 - \frac{T_f}{T_0}\right) \tag{7}$$

where L is the latent heat of fusion for pure ice (333.9 kJ/kg), c_w equals the specific heat of water (4.23 kJ °C^{-1} kg^{-1}), c_i equals the specific heat of ice (2.11 kJ °C^{-1} kg^{-1}), $T_f = \mu S$ is the freezing temperature of brine with salinity S, with μ equals 0.054°C/ppt, and T_o is the starting temperature of the ice.

[28] Mass balance observations showed more than 0.30 m of ice growth at the Seattle thermistor string between December and March. Combining this growth with temperature profiles of the newly grown ice and using equations (6) and (7), Q_L is equal to 83.7 MJ m^{-2}.

[29] The heat contributed from the ocean is computed from:

$$Q_w = \int F_w dt \tag{8}$$

where F_w is the ocean heat flux. Lacking specific data from SHEBA, we set F_w equal to a constant value of 2 W m^{-2} [*Maykut and Untersteiner*, 1971], but we recognize there is considerable uncertainty as to whether this choice is appropriate, and over what limits the value might have varied. Integrating equation (8) over the time period of interest gives Q_w equal to 15.6 MJ m^{-2}.

[30] Combining all the terms, the total heat extracted between 9 December 1997 and 8 March 1998 was 111 MJ m^{-2}. The largest contribution by far was from ice growth (75%), followed by the ocean heat flux (15%) and cooling of the ice (9%). The contribution from cooling of the snow was less than 1%.

[31] The temperature gradient in the snow was computed every hour using the air temperature (T_a), the snow–ice interface temperature (T_{si}), and the snow depth (H_s):

$$\frac{dT_s}{dz} = \frac{(T_a - T_{si})}{H_s} \tag{9}$$

[32] These hourly values were added together to approximate the integral in equation (4), which was then solved for the inferred effective bulk thermal conductivity of the snow. The result was 0.33 W m^{-1} K^{-1}. While this inferential estimate is approximate, the uncertainties are reduced by averaging over time. An error of 1 cm in ice growth would change k_s by 0.01, a 50% difference in the

Table 4. Effective Bulk Thermal Conductivity Computed From Ice Growth and Snow–Ice Interface Temperatures[a]

Gauge	Location	Initial ice thickness, cm	ΔIce thickness, cm	Initial snow depth, cm	Final snow depth, cm	k_s (eff. bulk, inferred), W m^{-1} K^{-1}
G7	Seattle-pond	104	47.9	32	39	0.299
G9	the "Ridge" site	271	51.1	28	15	0.388
G11	Baltimore	69	39.3	76	65	0.699
G21	the "Ridge" site	189	39.4	38	33	0.542
G34	Seattle-pond	164	34.0	23	26	0.237
G37	Baltimore	69	38.9	41	55	0.279
G39	Seattle-pond	114	39.0	34	31	0.255
G44	Seattle-hummock	223	43.0	4	2	0.290
G51	Baltimore	385	16.4	21	37	0.105
G57	the "Ridge" site	254	29.5	18	31	0.380
G58	the "Ridge" site	294	33.2	7	7	0.168
G63	Baltimore	151	39.1	38	63	0.469
G133	Baltimore	256	30.0	25	43	0.291
G142	Seattle-pond	130	37.0	31	38	0.387
G148	Baltimore	79	61.4	19	28	0.315
					average:	0.340
					std. deviation:	0.148

[a] For gauge numbers, refer to Figure 6.

specific heat of the ice would change k_s by 0.01, and an error in the value of the ocean heat flux of 1 W m^{-2} would change k_s by 0.02.

[33] We can expand the inferential analysis to those locations where we monitored the snow–ice interface temperature [*Sturm et al.*, 2001]. At the Seattle site, there were four such locations (Figure 6, marked); elsewhere an additional 26 sites were monitored, but of these only 11 have suitable time series of snow depth, ice thickness, and snow–ice interface temperature records for estimating the inferred effective bulk thermal conductivity. The nonuseable sites include locations where there were gaps in the snow depth and ice thickness records and nine sites near ridges where the ice thickness actually decreased over the winter. For purposes of computation, we use the same time period as before. Air temperatures are known to have been uniform at sites within a few kilometers of the SHEBA camp [*Claffey et al.*, 1999] [*Perovich and Elder*, 2001], so we have used the air temperature record from the Seattle site everywhere. Similarly, we have assumed that values of $Q_{ss'}$, $Q_{si'}$ and Q_w were also the same at all sites, though it is likely that Q_w was higher at ridge sites (one case only). We used the change in ice thickness observed at each site and equations (6) and (7) to compute Q_L. The measured interface temperature, combined with the Seattle air temperature, was used in equation (9) to approximate the temperature gradient in the snow. This gradient was integrated over the time period of interest, and the effective bulk value of k_s was computed as before.

[34] The results are listed in Table 4. Values range from a low of 0.168 to a high of 0.699 W m^{-1} K^{-1}, with an average value of 0.34 W m^{-1} K^{-1}, close to our previous inferential estimate from the Seattle thermistor string. We note that the three highest values fall well above any realistic value for seasonal snow and that only one value fell below the estimates based on needle probe measurements and snow pit stratigraphy.

[35] What is the basis of the mismatch between the two bulk estimates? One notable fact concerning the computed effective bulk thermal conductivity values listed in Table 4 are that they are poorly explained by snow depth ($r^2 = 0.20$) or the inverse of snow depth ($r^2 = 0.04$). A similar finding is obtained if we look at ice growth at all the stakes at the Seattle site. For these 22 stakes, ice growth varied from 0.24 to 0.75 m over the winter period, but the increase in ice thickness was only weakly related to the ice thickness, the snow depth, the inverse snow depth, or some combinations thereof (Table 5). Though both snow and ice were significant predictors of ice growth, snow alone explained only 32% of the variance in growth, the inverse snow depth explained only 11%, and snow depth and ice thickness combined explained just 46% of the variance, the other 54% coming from some other source. If we use a standard combined parameter for snow and ice thickness ($1/(k_s h_i + k_i h_s)$, with h indicating thickness, s for snow, i for ice) [*Maykut*, 1978], the explained variance is still low (33%). These observations, reinforced by the wide range of values in Table 4, suggest to us that ice growth is not vertically coupled to ice thickness or snow depth as strongly as is commonly assumed, at least at the scale of the Seattle site. These findings lead us to question whether a one-dimensional model of snow and ice is adequate for describing real snow and ice thermodynamics.

7. Nonvertical Transfer of Heat Due to Ice and Snow Geometry

[36] Using a time-dependent two-dimensional finite element (FE) model (FEHT, F-Chart Software: http://

Table 5. Ice Growth Regression Statistics: Multiple Regressions Used for Snow Depth and Ice Thickness Combined[a]

	n	r^2	F
ave. snow depth	22	0.25	6.79
max. snow depth	22	0.10	2.21
median snow depth	22	0.32	9.22
ave. snow depth and ice thickness	22	0.46	8.16
inverse ave. snow depth	22	0.11	3.72
inverse max. snow depth	22	0.07	2.68
inverse median snow depth	22	0.10	3.45
ave. inv. snow depth and ice thickness	22	0.12	2.49
$1/(k_s*h_i + k_i*h_s)$	22	0.33	11.33

[a] F indicates the F test for significance; F-critical in all cases was less than 0.01.

Table 6. FE Model Boundary Conditions and Input Parameters

Type of model:	Time-dependent heat transfer, finite element
Number of elements:	2219
Solution method:	Crank-Nicholson
Geometry:	See Figure 1
Upper (snow) surface:	Air temperature as represented by a third-order polynomial fit to real data
Lower (ice) surface:	Convective boundary, −2°C, Convective coeff. 20 W m^{-2} K^{-1}
Lateral surfaces:	No horizontal heat flux
Initial conditions:	Snow (−10°C), ice (−4°C)
Run length	15 October to 1 June
Snow properties	
Density, g cm^{-3}	0.33
Therm. cond., W m^{-1} K^{-1}	0.15
Specific heat, J kg^{-1} K^{-1}	2030
Ice properties	
Density, g m^{-3}	0.917
Therm. cond., W m^{-1} K^{-1}	2
Specific heat, J kg^{-1} K^{-1}	2030

www.fchart.com), we have simulated the heat flow through cross-section A−A′ in Figures 1 and 6. The model boundary conditions and input parameters are listed in Table 6. Model output was checked for accuracy by comparing simulated temperatures to measured temperatures at both the snow−ice interface and at depth in the ice. These generally agreed within 2°C. The results indicate that there was substantial lateral as well as vertical heat flow in the ice. Heat flowed away from refrozen ponds covered by thick snow and up through ice hummocks where there was little snow. The convergence of heat flow paths into hummocks extended as much as 7 m laterally from hummock centers (Figure 7), and at times during the winter the resultant heat flux was up to 5 times greater than the flux over adjacent ponds. The pattern was basically set by the snow and ice geometry and therefore did not vary much through time. As the air temperature varied, overall magnitudes of the flux changed, but heat

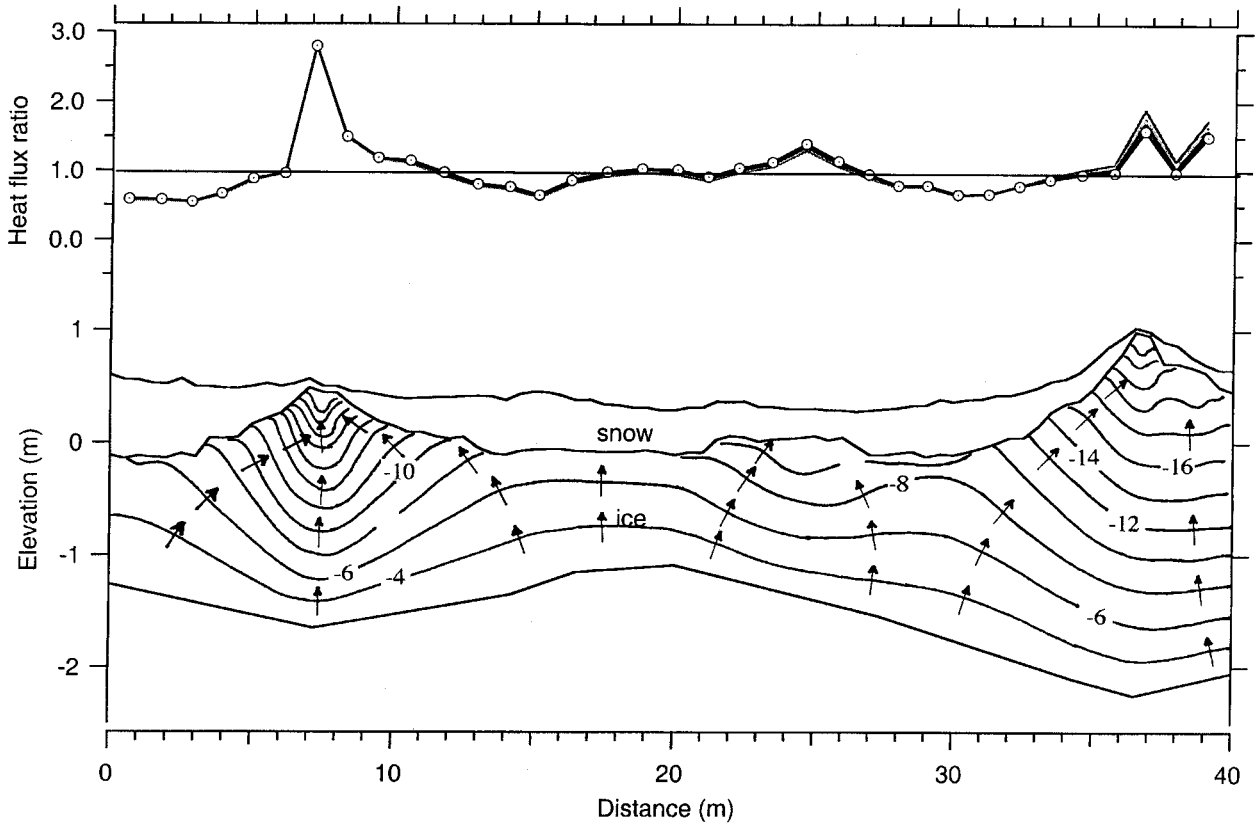

Figure 7. Isotherms (2°C contours) and heat flow paths (arrows) in the snow and ice at Seattle (lower), resulting in heat flux concentrations (upper) over ice hummocks. The heat flux ratio is the local vertical heat flux (over 1 m increments horizontally) divided by the average for the entire cross section.

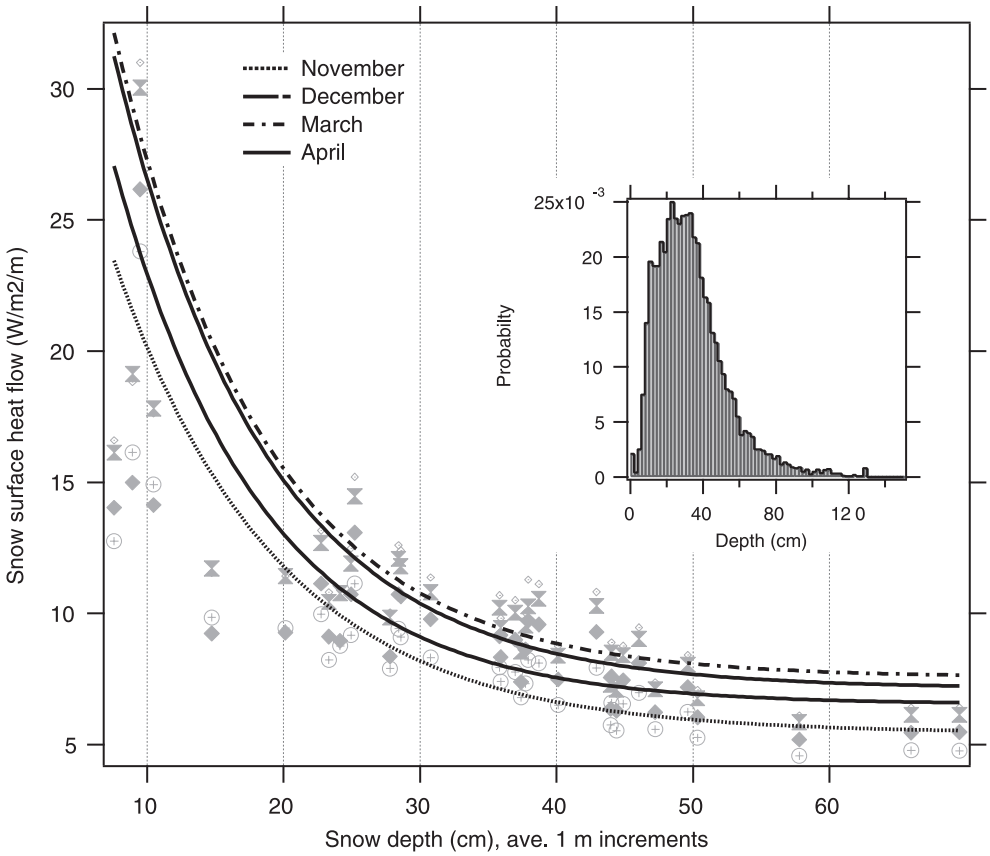

Figure 8. Vertical heat flux as a function of snow depth derived from a two-dimensional heat flow model of the cross section of snow and ice shown in Figure 7. The inset is the snow depth distribution for the SHEBA area determined by *Sturm et al.* [2002].

continued to flow away from ponds and toward ice hummocks.

[37] We can compare the vertical heat flux out of the top of the snow over ponds to that over hummocks by computing a heat flux ratio (the local vertical heat flux divided by the average vertical heat flux for the entire cross section) (Figure 7, top). Ponds with deep snow had values around 0.6, while hummocks with thin snow had values that ranged from 1.5 to 3. These ratios suggest the presence of concentrated ''hot spots'' at the snow ice surface where the rate of heat loss was much higher than elsewhere. In Figure 1 these ''hot spots'' might coincide with the shiny areas where the snow has melted away early. In a simple way, these ''hot spots'' can be thought of as arising where ice hummocks, 0.2 to 0.9 m high, have displaced a snow cover that was 10 to 15 times better a thermal insulator.

[38] Alternating melt ponds and ice hummocks were common at SHEBA and are common on the ice pack in general. Variations in snow depth (h_s) are even more pronounced in deformed ice areas. We think that heat loss from ''hot spots'' resulting from spatial variability in snow and ice geometry is potentially an important mechanism in the overall heat balance of the ice. Using the results of the FE model, we have tried to obtain an order of magnitude estimate of how much this mechanism might enhance the heat flow from a sizable (1 km^2) area of ice. From the cross sections in Figures 1 and 6 we have determined the vertical heat flux as a function of snow depth averaged over 1-m horizontal increments (Figure 8) at a number of times during the winter. Along this section, depth is a good indicator of whether there was a hummock or a pond beneath the snow. For snow depths in excess of 0.4 m (ponds), the flux was basically low and independent of depth, but as the snow became shallower, the heat flux increased rapidly. We approximate the increase using an exponential function ($a_0 + a_1 \exp\{-a_2 h_s\}$ where a_n indicates coefficients adjusted using a least squares process) because it captures the essential feature that a disproportionate amount of heat is lost through the thin snow areas. This is neither a general nor a universal function because the flux varies with the three-dimensional geometry of the ice and snow in a complex way we do not fully understand. Model results also show that the form of the function changes little through the winter (until the spring warming begins) because it is controlled primarily by the snow and ice geometry, not the air temperature forcing.

[39] The heat flow versus depth function can be convolved with a snow depth distribution function for the larger area around ice station SHEBA (Figure 8, inset) [see also *Sturm et al.*, 2002] to determine the enhancement in heat flow due to ''hot spots.'' The mean depth for SHEBA (n = 21,169) was 33.7 cm. For the cross sections in Figures 1 and 6 it was 30.2 cm, a reasonably close match. We apply the function in Figure 8 to a 1 km^2 snow covered area with a hypothetical depth distribution that matches the inset in Figure 8, and compare it to the flux for a similar area with a

homogeneous snow cover of 33.7 cm. The flux from the heterogeneous snow cover is 1.40 times greater. This implies that if we had applied a bulk thermal conductivity value of 0.14 to the area, we would have underestimated the heat flux by 40%. Alternately, it suggests that effective bulk thermal conductivity would need to be increased to 0.20 W m^{-1} K^{-1} to produce the correct areal average.

8. Discussion

[40] Most thermodynamic sea ice models use a bulk thermal conductivity value for snow of approximately 0.3 W m^{-1} K^{-1} [*Maykut and Untersteiner*, 1971; *Semtner*, 1976; *Ledley*, 1991; *Ebert and Curry*, 1993; *Wu et al.*, 1999] and a one-dimensional heat flow equation that is applied repetitively over the model domain. This traditional value can be traced back to the model of *Maykut and Untersteiner* [1971], who used a regression equation developed by Abel's [1891] and a density of 0.3 g cm^{-3} to determine k_s. This was a reasonable approach at the time, since no direct measurements from sea ice were available, but Abel's experimental technique (calculation of k_s using the ratio of the amplitude of diurnal fluctuations of the temperature at various levels in the snow) is difficult to apply accurately and is likely to have resulted in the inclusion of other heat transfer mechanisms besides conduction. His values of k_s are probably too high. Subsequent models, though employing more complex formulations for k_s [e.g., *Ledley*, 1991; *Ebert and Curry*, 1993], continue to use regressions that produce values closer to 0.3 than to the bulk value of 0.14 W m^{-1} K^{-1} we report here. Using the higher value, the models seem to obtain reasonable estimates of aggregate ice thickness, though this could be for many reasons. When lower values (0.16 W m^{-1} K^{-1}) are used, some model simulations result in considerably thinner ice [*Wu et al.*, 1999], while others predict minimal reduction [*Fichefet et al.*, 2000]. Similarly, as we have shown here, the value of k_s we infer from ice growth observations is closer to 0.3 than 0.14 W m^{-1} K^{-1}. What is the correct value? Why does the mismatch exist?

[41] We think the answer to this question is summarized in this quote by *Wu et al.* [1999]:

> "The snow cover over the sea ice is complex and highly variable. Because coupled climate models cannot explicitly include all the complexities, or such things as wind pumping through the snow, improved observations are needed to correctly parameterize the thermal conductivity of snow."

We would go further, suggesting that even at spatial scales considerably smaller than those used in climate models, temporal and spatial heterogeneity of the snow and ice system, lateral heat transport, and nonconductive heat transfer processes combine to enhance winter heat losses from the ocean to the atmosphere and raise the apparent value of k_s. We agree that there is a need to parameterize heat transfer across the snowpack for models at many scales, but we think these parameterizations should start with measured values of snow thermal conductivity, then add explicit enhancements due to spatial heterogeneity, scaling issues, and nonconductive heat transfer.

[42] We see no basis for discarding the direct measurements. The ones reported here, and a companion set from snow on Antarctic sea ice [*Sturm et al.*, 1998], have been acquired using a method we have carefully tested and critically evaluated. It appears to be the best method currently available for snow. The measurements include the vapor transport that is present in all natural snow covers, but exclude air convection. The scale of the test is on the order of the thickness of a layer of snow (Figure 2), about 0.1 to 0.2 m.

[43] Our second set of measurements, values of k_s inferred from the growth of ice, are probably also valid, but they represent *effective* values of k_s, because in this case we are aggregating over a much larger area. At this scale, lateral heat transport in the ice and snow, and possibly convection in the snow, operate and enhance the rate at which heat is removed from the ocean. Because we have assumed in our calculations (equations (4)–(9)) that all heat transport is vertical, any transport realized by alternate mechanisms must necessarily raise the apparent value of k_s. While the average effective value of k_s inferred from ice growth (0.34 W m^{-1} K^{-1} in Table 4) is close to the commonly assumed values in models, we think it is more important to note the wide range of values obtained from all the sites (std. dev.: 0.15 W m^{-1} K^{-1}). We believe this is evidence for effects of spatial heterogeneity on the heat flow. Likewise, the fact that we can only explain 46% of the observed ice growth at Seattle using the snow and ice thickness values from immediately above the location where the growth measurements were made (Table 5) suggests to us a lack of direct vertical coupling that argues for complex heat flow paths. Our FE model results suggest that the scale of lateral heat transport is on the order of 10 meters, which is consistent with the heterogeneity of the snow and ice system that can be seen in Figures 1 and 6.

[44] A crude estimate from the 2-D modeling (Figures 7 and 8) suggests that when scaling up to areas of tens to hundreds of meters, the average bulk value (0.14 W m^{-1} K^{-1}) should be increased at least 40% to 0.20 W m^{-1} K^{-1} to include the effect of horizontal heat transfer. This enhancement is not sufficient to fully close the gap between the directly measured value and the value inferred from ice growth, but it reduces the mismatch substantially. Snow textural variations could further enhance the geometric effects, and variations in snow depth associated with larger scale ice features (leads, ridges) would enhance winter heat losses still more.

[45] Buoyancy-driven convection may also contribute to the mismatch between the direct measurements of k_s and those inferred from ice growth. In needle probe tests, convection is precluded by limiting the length of the test or reducing the temperature rise at the needle, but in a natural snowpack, buoyancy-driven convection can occur if the layers are permeable enough and if they are subjected to strong enough temperature gradients. *Sturm* [1991] and *Sturm and Johnson* [1991] have shown that convection is prevalent in the subarctic snowpack, which contains a high percentage of extremely permeable depth hoar. Depth hoar layers at SHEBA (Figure 2) were comparable in density and texture to depth hoar layers found in the subarctic snowpack, and the temperature gradients were of similar magnitude. Unlike the subarctic snowpack, however, these depth hoar layers were capped by a dense wind slab with low permeability (Figure 2). If buoyancy-driven convection occurred, it would have been limited to layers "b," "c," and "d." The large spatial variability in temperatures at the

Table A1.

k_{ave}	Snow code	Density	Hardness	k_{ave}	Snow code	Density	Hardness
0.034	11	0.24	2	0.162	3	0.35	3
0.038	13	0.31	1	0.163	7	0.42	4
0.043	12	0.26	2	0.165	6	0.35	3
0.044	12	0.21	2	0.167	12	0.28	3
0.045	13	0.25	1	0.170	10	0.32	1
0.045	12	0.38	3	0.171	9	0.43	4
0.046	12	0.38	3	0.174	9	0.38	4
0.047	13	0.25	1	0.175	9	0.38	3
0.047	10	0.24	1	0.178	7	0.42	4
0.053	1	0.15	1	0.179	9	0.38	3
0.056	11	0.25	2	0.198	5	0.39	3
0.059	11	0.25	2	0.203	5	0.39	3
0.061	11	0.25	2	0.207	5	0.39	3
0.063	13	0.25	1	0.214	9	0.43	3
0.067	11	0.30	1	0.215	9	0.30	3
0.068	13	0.25	1	0.215	7	0.38	4
0.071	12	0.29	4	0.225	7	0.38	4
0.075	12	0.29	4	0.226	3	0.36	2
0.076	13	0.24	1	0.234	7	0.44	4
0.076	10	0.29	1	0.235	9	0.30	3
0.078	13	0.24	1	0.248	9	0.40	2
0.079	10	0.24	1	0.250	9	0.40	2
0.090	12	0.30	2	0.257	9	0.45	4
0.091	12	0.30	2	0.265	9	0.30	3
0.093	10	0.23	1	0.266	7	0.40	4
0.104	9	0.42	4	0.271	6	0.42	3
0.107	3	0.33	1	0.273	6	0.42	3
0.110	3	0.35	1	0.273	7	0.41	4
0.114	2	0.16	1	0.281	7	0.40	4
0.117	9	0.42	4	0.295	8	0.47	5
0.123	3	0.33	1	0.303	3	0.36	2
0.129	13	0.25	1	0.322	9	0.46	4
0.131	6	0.35	3	0.342	9	0.48	5
0.131	6	0.35	3	0.364	8	0.40	5
0.138	6	0.35	3	0.411	7	0.42	4
0.143	13	0.31	1	0.422	7	0.41	4
0.147	10	0.26	2	0.425	8	0.40	5
0.148	11	0.30	1	0.428	7	0.41	4
0.149	11	0.30	1	0.440	7	0.37	4
0.151	6	0.35	3	0.441	8	0.40	5
0.154	10	0.26	2	0.445	8	0.40	5
0.159	9	0.43	4	0.490	8	0.52	5
0.162	13	0.31	2	0.496	7	0.44	4
0.162	6	0.35	3	0.503	8	0.52	5
				0.574	15	0.58	6

All thermal conductivity measurements from SHEBA. For snow codes, see Table 2. Hardness is defined in the text

Layer	Snow code	Density	Hardness	k_h	k_c	k_{ave}
b	12	0.275	3	0.179	0.154	0.167
b	12	0.261	2	0.045	0.040	0.043
b	15	0.380	6	0.587	0.561	0.574
c	13	0.307	1	0.039	0.037	0.038
c	13	0.307	1	0.149	0.136	0.143
c	13	0.250	1	0.071	0.065	0.068
c	13	0.250	1	0.064	0.062	0.063
c	13	0.250	1	0.136	0.121	0.129
c	11	0.236	2	0.036	0.032	0.034
c	11	0.295	1	0.072	0.062	0.067
c	11	0.295	1	0.150	0.147	0.149
c	11	0.295	1	0.153	0.142	0.148
c	12	0.210	2	0.045	0.043	0.044
c	13	0.244	1	0.080	0.075	0.078
c	13	0.244	1	0.079	0.072	0.076
c	12	0.297	2	0.089	0.090	0.090
c	12	0.297	2	0.093	0.089	0.091
c	12	0.290	4	0.070	0.071	0.071
c	12	0.290	4	0.079	0.070	0.075
c	11	0.250	2	0.056	0.056	0.056
c	11	0.250	2	0.059	0.058	0.059
c	11	0.250	2	0.063	0.060	0.061
c	13	0.312	2	0.158	0.165	0.162
c	13	0.250	1	0.045	0.044	0.045

Table A1. (continued)

Layer	Snow code	Density	Hardness	k_h	k_c	k_{ave}
c	13	0.250	1	0.048	0.046	0.047
d	7	0.410	4	0.420	0.424	0.422
d	7	0.410	4	0.406	0.450	0.428
d	9	0.434	4	0.162	0.155	0.159
d	9	0.434	4	0.164	0.177	0.171
d	12	0.380	3	0.046	0.045	0.046
d	12	0.380	3	0.046	0.044	0.045
d	9	0.300	3	0.220	0.210	0.215
d	9	0.300	3	0.230	0.240	0.235
d	9	0.300	3	0.260	0.270	0.265
d	9	0.377	4	0.163	0.185	0.174
drift	6	0.350	3	0.131	0.130	0.131
drift	6	0.350	3	0.125	0.136	0.131
drift	6	0.350	3	0.135	0.141	0.138
drift	6	0.350	3	0.146	0.156	0.151
drift	6	0.350	3	0.157	0.173	0.165
drift	6	0.350	3	0.154	0.169	0.162
e	10	0.264	2	0.139	0.154	0.147
e	10	0.264	2	0.163	0.144	0.154
e	10	0.323	1	0.168	0.171	0.170
f	9	0.382	3	0.182	0.176	0.179
f	9	0.382	3	0.170	0.179	0.175
f	8	0.515	5	0.483	0.497	0.490
f	8	0.515	5	0.527	0.478	0.503
f	7	0.370	4	0.426	0.454	0.440
f	7	0.380	4	0.210	0.239	0.225
f	7	0.380	4	0.218	0.212	0.215
f	7	0.440	4	0.498	0.493	0.496
f	7	0.440	4	0.244	0.224	0.234
f	6	0.421	3	0.258	0.287	0.273
f	6	0.421	3	0.270	0.271	0.271
f	9	0.395	2	0.240	0.255	0.248
f	9	0.395	2	0.250	0.249	0.250
f	9	0.447	4	0.241	0.272	0.257
f	9	0.415	4	0.111	0.096	0.104
f	9	0.415	4	0.123	0.110	0.117
f	7	0.420	4	0.185	0.171	0.178
f	7	0.420	4	0.172	0.154	0.163
f	8	0.473	5	0.291	0.298	0.295
f	7	0.418	4	0.403	0.419	0.411
f	7	0.414	4	0.279	0.266	0.273
f	10	0.289	1	0.079	0.073	0.076
f	9	0.475	5	0.352	0.332	0.342
f	9	0.462	4	0.321	0.323	0.322
f	9	0.434	3	0.206	0.222	0.214
f	8	0.403	5	0.346	0.381	0.364
f	8	0.403	5	0.404	0.446	0.425
f	8	0.403	5	0.467	0.415	0.441
f	8	0.403	5	0.455	0.434	0.445
g	7	0.404	4	0.247	0.285	0.266
g	7	0.404	4	0.283	0.279	0.281
g	3	0.329	1	0.105	0.110	0.107
g	3	0.329	1	0.119	0.126	0.123
g	3	0.362	2	0.298	0.307	0.303
g	3	0.362	2	0.226	0.225	0.226
g	3	0.345	3	0.160	0.163	0.162
g	3	0.350	1	0.114	0.105	0.110
h	1	0.145	1	0.052	0.053	0.053
h	2	0.155	1	0.115	0.112	0.114
h	10	0.239	1	0.076	0.082	0.079
h	10	0.239	1	0.045	0.049	0.047
h	10	0.228	1	0.086	0.099	0.093
j	5	0.389	3	0.215	0.198	0.207
j	5	0.389	3	0.190	0.206	0.198
j	5	0.389	3	0.212	0.194	0.203

base of the SHEBA snowpack (Perovich and Elder, submitted manuscript; Sturm, submitted manuscript) could facilitate thermal convection in the porous depth hoar layers. *Sturm* [1991] found that convection increased the effective thermal conductivity by a factor of 2 to 3, depending on the airflow velocity in the snow. If we apply this increase to layers "b," "c," and "d" and recalculate, the average bulk conductivity increases to about 0.22 (for a 2X increase) to about 0.25 W m^{-1} K^{-1} (for a 3X increase). These values, while closing the gap between direct and

inferred measurements, are speculative. First, convection tends to occur during periods of low air temperatures and diminishes when the temperature rises, making its overall contribution to the heat flow hard to assess. Second, little is known about convection in snow layers capped above by nearly impermeable snow, and below by sea ice.

[46] Forced convection by wind pumping seems unlikely to have affected the snowpack at SHEBA. As discussed by *Waddington and Harder* [1996] and *Albert et al.* [1996], in a windy environment like SHEBA, the near-surface permeability of the snow is rapidly reduced when saltating snow grains are deposited and clog surface pores. The resulting slabs are typically too impermeable to allow much airflow, and as a consequence, the wind has little impact on temperatures in the snow. During much of the winter of 1997–1998 at SHEBA, any potential wind pumping would have been limited by the presence of slab layers "d," "f," "g," and "j" (Figure 2). In addition, *Colbeck* [1989] has identified that wind pressure perturbations over surface dunes and drifts are likely to produce the most vigorous wind pumping, but most of the airflow is thought to occur within the upper part of the dunes and drifts, limiting the effectiveness of the wind pumping in moving heat.

9. Guidance to Modelers and Further Studies

[47] Based on our results, we would suggest the following when modeling the thermal properties of the snow cover on Arctic sea ice:

1. Use a metamorphic (Figure 5) rather than density-driven relationship (Figure 4) to determine the thermal conductivity of the snow on the sea ice of the Arctic Ocean. As pointed out elsewhere [*Sturm et al.*, 2002], the density of the snowpack on the Arctic sea ice does not change much with time. Neither depth hoar nor wind slabs (Figure 2) undergo much densification. The snow thermal properties, however, do evolve with time as the snow metamorphoses into depth hoar or is reworked by the wind. The trajectories in Figure 5 capture this evolution better than using a viscosity-based snow densification formula.

2. Use an effective conductivity composed of a base value of thermal conductivity (k_s = 0.14 W m^{-1} K^{-1} for SHEBA), and enhancement factors to account for spatial variations in heat flow or convection. *Fourier* [1822] defined thermal conductivity as the proportionality constant between temperature gradient and heat flow for a one-dimensional system. By defining the conductivity as consisting of a base plus enhancement, a clear distinction can be made between what portion of the heat flow is the result of truly one-dimensional conductive processes, and what portion is the result of more complicated processes like lateral heat flow or convection. Many of the heat transfer enhancement processes (e.g., wind pumping) do not scale with the temperature gradient. The model results may be the same, but this more flexible approach might allow our understanding of the processes to improve.

Appendix A: 89 Thermal Conductivity Measurements

[48] All snow thermal conductivity measurements made at SHEBA (see Table A1).

[49] **Acknowledgments.** We thank the crew of the Canadian Coast Guard icebreaker Des Groseilliers along with the logistics group from the University of Washington Applied Physics Laboratory for their superb support during the SHEBA field program. B. Elder, J. Richter-Menge, W. B. Tucker III, T. Udall, H. Eiken, T. Grenfell, and B. Light assisted in collecting snow measurements. We thank R. E. Moritz for allowing us to use meteorological data collected during SHEBA and William Lipscomb and two anonymous reviewers for their valuable comments on earlier drafts of this paper. The work was funded by the National Science Foundation Office of Polar Programs and the Office of Naval Research High Latitude Physics Program.

References

Abel's, G., Beobachtungen der Tglichen Periode der Temperatur im Schnee und Bestimmung des Warmeleitungsvermogens des Schnees als Function Seiner Dichtigkeit (Observations of daily temperature variations in a snow cover) (in German), *Repert. Meteorol. Herausgegeben Kaiserlichen Akad. Wiss.*, *16*, 1–53, 1893.

Albert, M. R., E. M. Arons, and R. E. Davis, Firn properties affecting gas exchange at Summit, Greenland: Ventilation possibilities, in *NATO ASI Ser. 1: Chemical Exchange Between the Atmosphere & Polar Snow*, edited by E. W. Wolff and R. C. Bales, pp. 500–530, Springer-Verlag, 1996.

Blackwell, J. H., The axial-flow error in the thermal-conductivity probe, *Can. J. Phys.*, *34*, 412–417, 1956.

Brun, E., P. David, M. Sudul, and G. Brunot, A numerical model to simulate snow-cover stratigraphy for operational avalanche forecasting, *J. Glaciol.*, *38*, 13–22, 1992.

Claffey, K. J., E. L. Andreas, D. K. Perovich, C. W. Fairall, P. S. Guest, and P. O. G. Perrson, Surface temperature measurements at SHEBA, *Fifth Conference on Polar Meteorology and Oceanography, Dallas*, Am. Meteorol. Soc., 1999.

Colbeck, S. C., Air movement in snow due to windpumping, *J. Glaciol.*, *35*, 209–213, 1989.

Colbeck, S., E. Akitaya, R. Armstrong, H. Gubler, J. Lafeuille, K. Lied, D. McClung, and E. Morris, *The International Classification for Seasonal Snow on the Ground*, 23 pp., The International Commission on Snow and Ice of the International Association of Scientific Hydrology/International Glaciological Society/U.S. Army CRREL, IASH Report MP 2794, 1992.

Colony, R., V. Radionov, and F. J. Tanis, Measurements of precipitation and snowpack at Russian North Pole drifting stations, *Polar Rec.*, *34*, 3–14, 1998.

DeVries, D. A., Simultaneous transfer of heat and moisture in porous media, *Eos Trans. AGU*, *39*, 909–916, 1958.

DeVries, D. A., and A. J. Peck, On the cylindrical probe method of measuring thermal conductivity with special reference to soils, II, Analysis of moisture effects, *Aust. J. Phys.*, *11*, 409–423, 1958.

Ebert, E. E., and J. A. Curry, An intermediate one-dimensional thermodynamic sea ice model for investigating ice–atmosphere interactions, *J. Geophys. Res.*, *98*, 10,085–10,109, 1993.

Ewen, J., and H. R. Thomas, The thermal probe: A new method and its use on an unsaturated sand, *Geotechnique*, *37*, 91–105, 1987.

Fichefet, T., B. Tartinville, and H. Goossee, Sensitivity of the Antarctic sea ice to the thermal conductivity of snow, *Geophys. Res. Lett.*, *27*, 401–404, 2000.

Fourier, J. B. J., *The Analytical Theory of Heat*, translated, with notes, by A. Freeman, Dover, Mineola, N. Y., reprinted 1955, 1822.

Jaafar, H., and J. J. Picot, Thermal conductivity of snow by a transient state probe method, *Water Resour. Res.*, *6*, 333–335, 1970.

Jaeger, J. C., Conduction of heat in an infinite region bounded internally by a circular cylinder of a perfect conductor, *Aust. J. Phys.*, *9*, 167–179, 1956.

Jaeger, J. C., The measurement of thermal conductivity and diffusivity with cylindrical probes, *Eos Trans. AGU*, *39*, 708–712, 1958.

Jordan, R., *One-Dimensional Temperature Model for a Snow Cover; Technical Documentation for SNTHERM.89*, 49 pp., U.S. Army Cold Regions Research and Engineering Laboratory, Special Report ADA-245, 1991.

Lachenbruch, A. H., A probe for measurements of thermal conductivity of frozen soils in place, *Eos Trans. AGU*, *38*, 691–697, 1957.

Lange, M., Measurement of thermal parameters in Antarctic snow and firn, *Ann. Glaciol.*, *6*, 100–104, 1985.

Ledley, T. S., Snow on sea ice: Competing effects in shaping climate, *J. Geophys. Res.*, *96*, 17,195–17,208, 1991.

Lide, D. R., *CRC Handbook of Chemistry and Physics*, pp. 6–8, CRC Press, 1997.

Maykut, G. A., Energy exchange over young sea ice in the central Arctic, *J. Geophys. Res.*, *83*, 3646–3658, 1978.

Maykut, G. A., and N. Untersteiner, Some results from a time-dependent thermodynamic model of sea ice, *J. Geophys. Res.*, *76*, 1550–1575, 1971.

Mellor, M., Engineering properties of snow, *J. Glaciol.*, *19*, 15–66, 1977.

Murakami, S., and N. Maeno, Thermal conductivity of snow and snow/metal mixtures (in Japanese with English abstract), *Low Temp. Sci., Ser. A*, *48*, 13–24, 1989.

Ono, N., Specific heat and heat of fusion of sea ice, in *International Conference on Low Temperature Science, Sapporo, 14–19 August 1966, Proceedings, Vol. 1, Part 1*, pp. 599–610, Inst. of Low Temp. Sci., Hokkaido Univ., 1967.

Perovich, D. K., and B. C. Elder, Temporal evolution of Arctic sea-ice temperature, *Annal. Glaciology*, *33*, 207–211, 2001.

Perovich, D. K., et al., Year on ice gives climate insights, *Eos Trans. AGU*, *80*, 481–486, 1999.

Pitman, D., and B. Zuckerman, Effective thermal conductivity of snow at −88°, −27° and −5°C, *J. Appl. Phys.*, *38*, 2698–2699, 1967.

Pratt, A. W., Heat transmission in low conductivity materials, in *Thermal Conductivity*, edited by R. P. Tye, pp. 301–405, Academic, 1969.

Presley, M. A., and P. R. Christensen, Thermal conductivity measurements of particulate materials: A review, *J. Geophys. Res.*, *102*, 6535–6549, 1997.

Radionov, V. F., N. N. Bryazgin, and E. I. Alexandrov, *The Snow Cover of the Arctic Basin*, APL-UW-TR 9701, 95 pp., Appl. Phys. Lab., Univ. of Wash., 1997.

Schwerdtfeger, P., The thermal properties of sea ice, *J. Glaciol.*, *4*, 789–807, 1963.

Semtner, A. J. J., A model for the thermodynamic growth of sea ice in numerical investigations of climate, *J. Phys. Oceanogr.*, *6*, 379–389, 1976.

Sturm, M., *The Role of Thermal Convection in Heat and Mass Transport in the Subarctic Snow Cover*, 84 pp., USA-CRREL, Research Report 91-19, 1991.

Sturm, M., and J. B. Johnson, Natural convection in the subarctic snow cover, *J. Geophys. Res.*, *96*, 11,657–11,671, 1991.

Sturm, M., J. Holmgren, M. König, and K. Morris, The thermal conductivity of seasonal snow, *J. Glaciol.*, *43*, 26–41, 1997.

Sturm, M., K. Morris, and R. Massom, The winter snow cover of the west Antarctic pack ice: Its spatial and temporal variability, in *Antarctic Sea Ice Physical Processes, Interactions and Variability*, edited by M. O. Jeffries, pp. 1–18, Am. Geophys. Union, 1998.

Sturm, M., J. Holmgren, and D. K. Perovich, Spatial variations in the winter heat flux at SHEBA: Estimates from snow-ice interface temperatures, *Annal. Glaciol.*, *33*, 213–220, 2001.

Sturm, M., J. Holmgren, and D. K. Perovich, The winter snow cover on the sea ice of the Arctic Ocean at SHEBA: Temporal evolution and spatial variability, *J. Geophys. Res.*, *107*, 10.1029/2000JC000400, in press, 2002.

Touloukian, Y. S., P. E. Liley, and S. C. Saxena, *Thermal Conductivity: Nonmetallic Liquids and Gases*, *3*, Plenum, New York, 1970.

Vowinkel, E., and S. Orvig, The climates of the North Polar Basin, in *Climates of the Polar Region*, edited by S. Orvig, pp. 129–226, Elsevier Sci., 1970.

Waddington, E. D., and S. L. Harder, The effects of snow ventilation on chemical concentrations, in *NATO ASI Ser.: Chemical Exchange Between the Atmosphere & Polar Snow*, edited by E. W. Wolff and R. C. Bales, pp. 403–451, Springer-Verlag, 1996.

Warren, S. G., V. F. Radionov, N. N. Bryazgin, Y. I. Aleksandrov, and R. Colony, Snow depth on Arctic sea ice, *J. Clim.*, *12*, 1814–1829, 1999.

Wu, X., W. F. Budd, V. I. Lytle, and R. A. Massom, The effect of snow on Antarctic sea ice simulations in a coupled atmosphere–sea ice model, *Clim. Dyn.*, *15*, 127–143, 1999.

J. Holmgren and M. Sturm, U.S. Army Cold Regions Research & Engineering Laboratory-Alaska, P.O. Box 35170, Fort Wainwright, AK 99703-0170, USA. (msturm@crrel.usace.army.mil)

D. K. Perovich, U.S. Army Cold Regions Research & Engineering Laboratory, 72 Lyme Road, Hanover, NH 03755, USA.